Journal of Magnetism and Magnetic Materials 361 (2014) 81–87

Contents lists available at ScienceDirect

Journal of Magnetism and Magnetic Materials

journal homepage: www.elsevier.com/locate/jmmm

Low temperature neutron diffraction study of $Nd_{1-x}Sr_xCrO_3$ ($0.05 \le x \le 0.15$)

Keka R. Chakraborty [a,*], S. Mukherjee [b], S.D. Kaushik [c], S. Rayaprol [c], C.L. Prajapat [d], M.R. Singh [d], V. Siruguri [c], A.K. Tyagi [b], S.M. Yusuf [a]

[a] Solid State Physics Division, Bhabha Atomic Research Centre, Mumbai 400085, India
[b] Chemistry Division, Bhabha Atomic Research Centre, Mumbai 400085, India
[c] UGC-DAE Consortium for Scientific Research – Mumbai Centre, R-5 Shed, BARC Campus, Trombay, Mumbai 400085, India
[d] Technical Physics Division, Bhabha Atomic Research Centre, Mumbai 400085, India

ARTICLE INFO

Article history:
Received 15 October 2012
Received in revised form
11 November 2013
Available online 19 February 2014

Keywords:
Neutron diffraction
Neutron scattering in condensed state matter
Magnetic susceptibility in magnetically ordered material
Magnetization
Magnetic ordering general theory and model

ABSTRACT

Low temperature magnetic structure of Sr substituted $NdCrO_3$ has been investigated using neutron diffraction in the temperature range of 2–300 K. We carried out a low temperature magnetization study in the temperature range 5–300 K. The Rietveld analysis of neutron diffraction patterns led us to conclude that the Cr moments have a $\mathbf{G_y}$ type of alignment of spins while the Nd moments align in a $-\mathbf{C_z}$ type fashion for all three samples. The weighted average $Cr^{3+/4+}$ ions moments were 3.19(7), 2.77(3) and 2.57(7) μ_B close to its theoretical Cr^{3+} moment value namely 3 μ_B at 2 K for the $x=0.05$, 0.1 and 0.15 samples respectively. While the Nd^{3+} moments for the three samples at 2 K were 3.0(1), 2.39(8) and 2.2(2), respectively.

1. Introduction

Rare-earth (*RE*) transition-metal (*TM*) oxides with perovskite structure have been a subject of renewed interest in relation to their practical uses as they have interesting properties like multiferroicity, colossal magnetoresistance, and high critical temperature superconductivity [1]. *RE*MnO_3 compounds have been studied extensively due to their interesting strong coupling between charge, spin, and lattice which leads to interesting properties like colossal magnetoresistance. Multiferroicity has been observed in some specific *RE*FeO_3 and more commonly in *RE*MnO_3 [2] compounds. The structural magnetic and electrical properties of all the *RE*CrO_3 compounds have also been investigated. The dependence of resistivity on temperature and polarization of chromites $DyCrO_3$, $HoCrO_3$, $YbCrO_3$ and $LuCrO_3$ was predicted to show ferroelectricity due to distorted CrO_6 polyhedra [3–7]. $LaCrO_3$ has been found to be highly conductive at high temperatures, a useful property with potential application in fuel cells [8,9]. Some of the refractory *RETMO*$_3$ perovskite materials in which either *RE* or *TM* sites are substituted with cations of acceptor- or donor-type, exhibit relatively high electrical conductivities at elevated temperatures. Hence, there has been considerable interest in these materials as high-temperature electrochemical devices. Many investigations on $LaCrO_3$, $YCrO_3$ and $NdCrO_3$ perovskite systems, have been focused on pure and doped materials of the former two but not much attention has been given to the sintering behavior and electrical conductivity of $NdCrO_3$ [10]. This compound has been prepared by various techniques, for example solid-state reaction, co-precipitation, simultaneous crystallization, and combustion synthesis methods. $NdCrO_3$, as well as other lanthanide chromites, unfortunately show poor sinterability and are very difficult to densify under atmospheric conditions [10–14]. Tripathi [15] and Tripathi and Lal [16] studied the electrical conductivity of $NdCrO_3$ with a low relative density and found that the value was as low as 0.7 S-m^{-1} at 800 °C. Others like Palguev et al. [17] synthesized $(Nd_{0.8}Ca_{0.2})CrO_3$ and they showed the electrical conductivity of 436 S-m^{-1} at 1000 °C in a wet hydrogen atmosphere (2.5% H_2O). There have been two heating steps for the synthesis of dense $LaCrO_3$ and $YCrO_3$ materials with high electrical conductivities [18,19] by sintering under reduced pressure and then annealing in air in order to fully oxidize the samples. Recently a work [20] on Sr doped $NdCrO_3$ found this material to show improvement in density and sinterability with increase in Sr doping level.

$NdCrO_3$ crystallizes in an orthorhombic structure conforming to space group *Pnma*. The Nd^{3+} ions are located in the spaces between CrO_6 octahedra. Magnetic ordering of Cr^{3+} ions occurs

* Corresponding author.
E-mail address: kekarc@barc.gov.in (K.R. Chakraborty).

http://dx.doi.org/10.1016/j.jmmm.2014.02.018
0304-8853

below the Néel temperature T_N=219 K [21]. The magnetic structure is G-type antiferromagnetic whereby each Cr^{3+} ion is antiferromagnetically aligned with all its nearest Cr^{3+} ion neighbors. There is a spin reorientation of Cr spins at 35 K. There are however very few reports on magnetic structure of doped $NdCrO_3$ [22]. The substitutions on $RETMO_3$ compounds result in changes to crystal field and hence, *RE* and *TM* ions interactions. The *TM–TM*, *RE–TM* and *RE–RE* interactions were found to be in a descending order, depending on the electron configuration, bonding strength, bond lengths and bond angles. In this study, we decided to investigate Sr doped $NdCrO_3$ for its structural and magnetic properties as this material has been found to be a good SOFC interconnect material [21]. The sinterability of Sr doped $NdCrO_3$ increases with increasing Sr content and the materials have a good electrical conductivity at high temperatures. Also, the solid solution having composition $Nd_{0.75}Sr_{0.25}CrO_3$ has a thermal expansion coefficient close to yttria stabilized zirconia and hence, is useful as an interconnect material [22]. The ionic size of Sr^{2+} is 1.32 Å which is different from Nd^{3+} 1.27 Å and it does not possess a magnetic moment. Hence it can be used to study the effect of non-magnetic atom substitution on magnetic properties of the parent compound and gives us a good handle to provide direct evidence of interactions among the magnetic cations.

As the low temperature magnetic structure of Sr doped $NdCrO_3$ compounds is not known, it is pertinent to carry out neutron diffraction measurements on these compounds.

2. Experimental

Samples of Sr^{2+} doped $NdCrO_3$ were prepared with stoichiometric amounts of heat activated Nd_2O_3, $Sr(NO_3)_2$, $Cr(NO_3)_3 \cdot 9H_2O$. The solids were dissolved in 1:1 aqueous nitric acid by slight warming. In each case, required amount of glycine was added, adjusting the nitrate to glycine ratio as 1:2. The solution so formed was heated to 100 °C on a hotplate to get a glassy, brownish colored gel. Temperature was then raised to 200 °C in order to have the combustion reaction to form a fluffy powder. The powder was initially calcinated at 800 °C for 4 h in a muffle furnace. Then the powders were made into pellets and heated at 1350 °C for 4 h in a Carbolite make furnace. $Nd_{1-x}Sr_xCrO_3$ (x=0.05, 0.10, 0.15) compounds are very hard, having glossy surface and difficult to powder again.

X-ray diffraction (XRD) studies were carried out using a Philips X-ray diffractometer. XRD data were recorded on samples for x=0, 0.05, 0.1 and 0.15. All samples showed good fits to the orthorhombic perovskite structure. The samples with $x > 0.15$ showed traces of impurities even after heat treatments and were not investigated further.

Magnetic properties of $Nd_{1-x}Sr_xCrO_3$ (x=0.0, 0.05, 0.10) were studied using a commercial Magnetic Properties Measurement (MPMS) system. The Focusing Crystal Diffractometer of UGC-DAE CSR Mumbai Center at the National Facility for Neutron Beam Research (NFNBR) Dhruva reactor, Mumbai (India), was used to

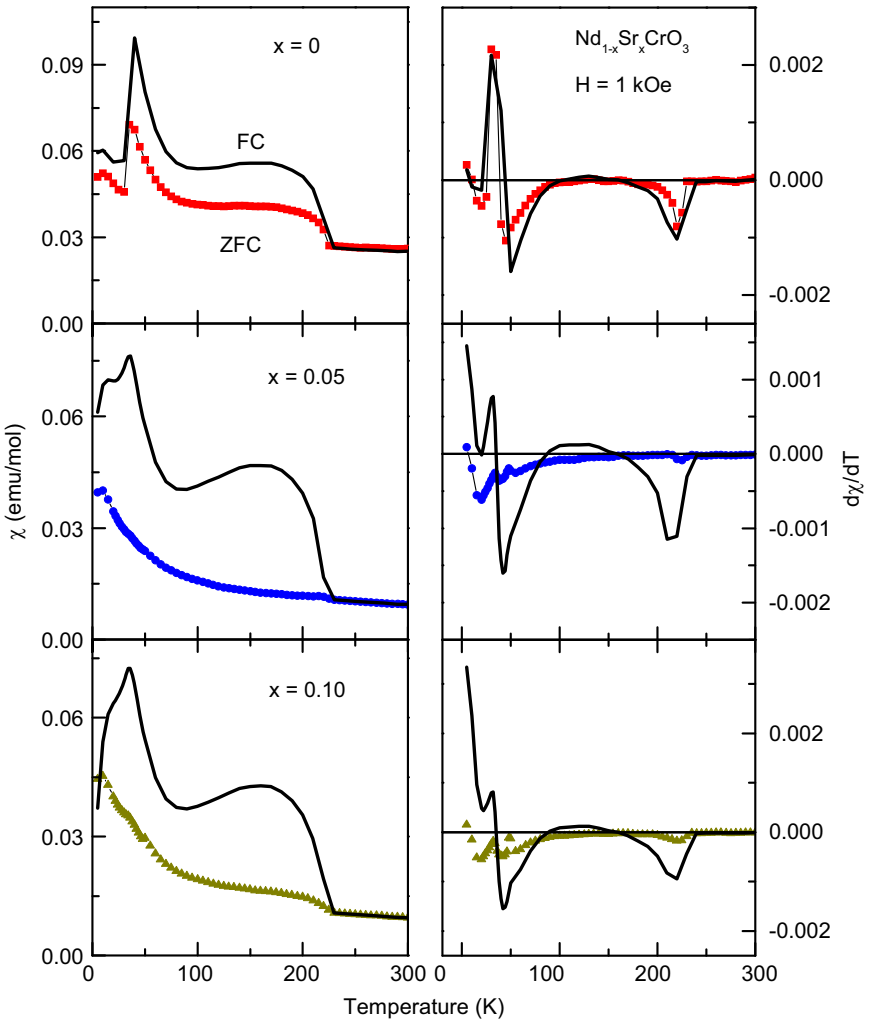

Fig. 1. Magnetic susceptibility and the first derivative of susceptibility as a function of temperature for the three samples x=0, 0.05 and 0.1.

record neutron diffraction data for all the samples in the range of 2–300 K at a wavelength of 1.48 Å. Powder samples were filled in vanadium cans which were then loaded in a *Cryogenics* make cryogen free magnet (CFM) system for temperature variation. The ND patterns were recorded in the warming cycle and analyzed using the Rietveld method and the refinement of both crystal and magnetic structures was carried out using the FULLPROF program [23].

3. Results and discussion

3.1. Magnetization

It is well known in the literature [21] that $NdCrO_3$ exhibits two ordering temperatures. One is the antiferromagnetic ordering (T_N) due to Cr^{3+} and the other due to Nd^{3+} ordering ($T_{RE}=T_{Nd}$). There is also another spin-reorientation temperature (T_{SR}) due to the reorientation of Cr spins. The ordering of the Nd^{3+} ions is known to be induced by the Cr^{3+} sublattice [25,26]. Therefore, the dilution of Nd^{3+} site by non-magnetic Sr^{2+} is likely to influence T_{RE}. Substitution of Sr^{2+} for Nd^{3+} results in Cr^{3+} to Cr^{4+} conversion due to charge compensation [21]. Du et al., [26] have experimentally shown that magnetic interactions between Nd–Cr in perovskite La doped $NdCrO_3$ are weakened with La dilution. Similarly, it can also be expected that the Nd–Cr magnetic interaction can be weakened by Sr substitution, and at the same time, the conversion of Cr^{3+} to Cr^{4+} due to charge compensation, may further lead to weakening of magnetic interactions or influence the magnetic structure.

In Fig. 1, the magnetic susceptibility ($\chi=M/H$) is plotted as a function of temperature for three samples of $Nd_{1-x}Sr_xCrO_3$ series. Magnetic susceptibility $\chi(T)$ has been measured in zero field cooled (ZFC) and field cooled (FC) states of the samples. Magnetization has been recorded while warming the sample. The first derivative of magnetic susceptibility is also shown in the right column for the corresponding sample, to highlight the phase transition temperatures. From the plot of $\chi(T)$ for $x=0.0$ sample, the two characteristic temperatures can be clearly seen at $T_N=220$ K and $T_{SR}=35$ K in the ZFC curve. On further decreasing the temperature, one more peak is seen around 10 K. This is more clearly evident in the plot of $d\chi/dT$ versus T. The third transition around 10 K is attributed to the ordering of Nd moments (T_{Nd}). The plot of FC $\chi(T)$ for $x=0$ sample is also shown in the same panel for direct comparison. Qualitatively, ZFC and FC show anomalies at identical temperatures; however ZFC–FC bifurcation takes place in the vicinity of T_N. Below T_N, the bifurcation becomes wider, indicating strong magnetic anisotropy in this system. With increasing Sr content, the T_N remains the same, there is no T_{SR}. However, the magnitude of the moment is weaker in the ZFC case. Sharp features of T_N and T_{SR} can be seen in the FC case, though. This observation further gives credence to strong magnetic anisotropy of the system. It is interesting to note from the plots of $d\chi/dT$ versus T, that T_{Nd} remains around 10 K for all the three compositions, which means that Sr substitution has little effect on the Nd ordering temperature, and hence can be attributed to the interaction between Nd and Cr sublattice [25]. This means that the changes observed in the magnetization behavior due to Sr doping in $NdCrO_3$ can be attributed to change in Cr^{3+} to Cr^{4+} with increasing Sr^{2+} content.

The Sr doped compounds exhibited a Curie–Weiss behavior between room temperature (300 K) and T_N ($T>220$ K). By carrying out the fitting of the Curie–Weiss law in this linear region, the paramagnetic Curie temperature (θ_p) and the effective Bohr magnetron number (μ_{eff}) were calculated. For the $x=0.05$ sample, the extrapolated θ_p temperature was 302 K. The paramagnetic moment (μ_{eff}) of this sample was 6.74 μ_B. For the $x=0.10$ sample, the values of θ_p and μ_{eff} were 340 K and 6.98 μ_B, respectively.

3.2. Neutron diffraction

Neutron diffraction data were recorded at a series of temperatures from 2 K to 300 K for the $x=0.1$ sample. Figs. 2 and 3 depict the Rietveld refined neutron diffraction patterns for $x=0.05$, 0.1, and 0.15 samples at 300 K and 2 K respectively All the peaks in the diffraction pattern were indexed in the *Pbnm* space group except for the peaks at scattering angle $2\theta \sim 15.5$ and 15.7, which are shown later to be due to purely magnetic ordering of Nd ions. Parameters for the three studied samples as well as goodness of fits at 2 K and 300 K are listed in Tables 1 and 2. Oxygen occupancy was varied during the refinement. It was observed that there was no oxygen deficiency within error limits. Hence, moments are influenced entirely by hole doping. Care was taken that no highly correlated parameters were refined simultaneously. In all the low temperature neutron diffraction patterns, certain regions in the diffraction patterns (60–65°) were excluded from refinement due to contamination from the cryostat shroud.

Upon analysis of neutron diffraction pattern, cell parameters were determined. The cell constants of the three samples recorded at 2 K show a rise from $x=0.05$ to $x=0.1$ and then a decrease for the sample with $x=0.15$. The rise is due to the fact that at low doping levels, bigger Sr^{2+} ions with radii 1.32 Å (in dodecahedral coordination) replace the smaller Nd^{3+} ions with radii 1.27 Å. But, on further doping with Sr^{2+}, a larger proportion of Cr^{3+} ions is converted to Cr^{4+} ions and as the radius of Cr^{4+} in a six fold coordination is 0.55 Å and that of Cr^{3+} ions is 0.615 Å, there is a drop in cell volume that compensates the expansion of unit cell. The cell constants at RT reduce with increasing doping level of Sr. As $NdCrO_3$ crystallizes in an orthorhombic cell, in space group *Pbnm* (or *Pnma*, no. 62 of the International Crystallographic Tables), Nd atoms are located at site 4*c* with site symmetry *m*, Cr atoms are located at site 4*b* and site symmetry 1^-, and O atoms are located at sites 4*c* and 8*d* with symmetry *m* and 1, respectively.

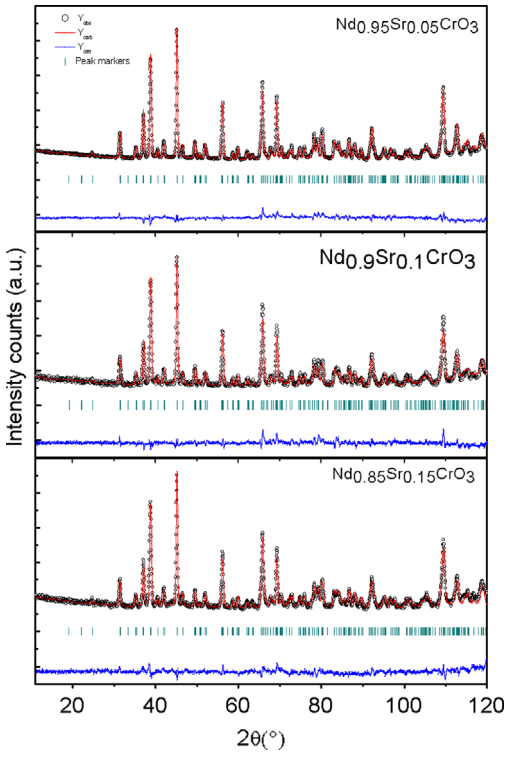

Fig. 2. Neutron diffraction patterns, (open black circles) observed data points, (continuous red line) calculated, and (blue continuous line) difference, patterns for the $x=0.05$, 0.1 and 0.15 samples at 300 K. (For interpretation of the references to color in this figure legend, the reader is referred to the web version of this article.)

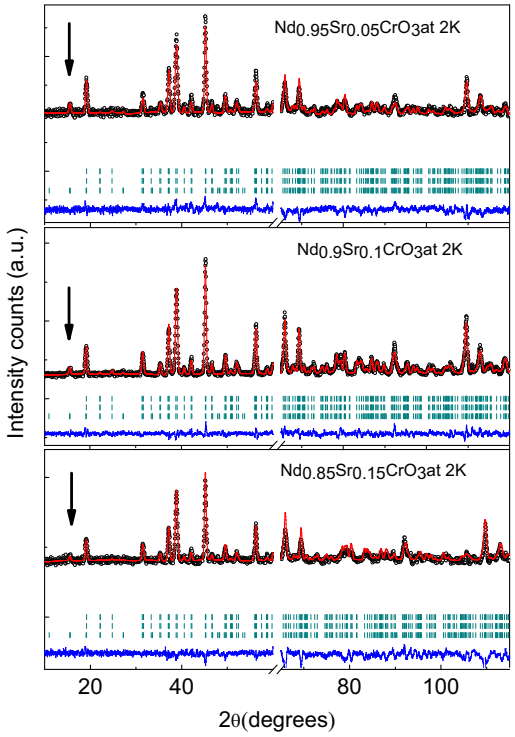

Fig. 3. Neutron diffraction patterns, (open black circles) observed data points, (continuous red line) calculated, and (blue continuous line) difference, patterns for the $x=0.05$, 0.1 and 0.15 samples at 2 K. (For interpretation of the references to color in this figure legend, the reader is referred to the web version of this article.)

Table 1
Structural parameters for $Nd_{1-x}Sr_xCrO_3$ ($x=0.05$, 0.1 and 0.15) samples at 300 K obtained from the Rietveld analysis of the neutron diffraction data.

Sample name	$Nd_{0.95}Sr_{0.05}CrO_3$	$Nd_{0.9}Sr_{0.1}CrO_3$	$Nd_{0.85}Sr_{0.15}CrO_3$
Space group	*Pbnm* (no. 62)		
Nd/Sr			
x	−0.0019(9)	−0.002(1)	−0.002(1)
y	0.0396(4)	0.0378(5)	0.0358(5)
z	0.25	0.25	0.25
B_{iso}	0.47(3)	0.19(4)	0.1(4)
SOF	0.95/0.05	0.9/0.1	0.85/0.15
Cr (1/2, 0, 0)			
B_{iso}	0.34(6)	0.1	0.1
SOF	1.0	1.0	1.0
O_1			
x	0.0765(9)	0.069(1)	0.062(1)
y	0.4834(6)	0.4856(7)	0. 4842(7)
z	0.25	0.25	0.25
B_{iso}	0.27(5)	0.03	0.63(7)
SOF	1.0	1.0	1.0
O_2			
x	0.7141(5)	0.7142(2)	0.7140(6)
y	0.2893(5)	0.2906(5)	0.2906(5)
z	0.0417(4)	0.0413(5)	0.0431(5)
B_{iso}	0.82(4)	0.57(5)	0.3(4)
SOF	2.0	2.0	2.0
a (Å)	5.4254(5)	5.4248(5)	5.4196(5)
b (Å)	5.4687(4)	5.4664(4)	5.4666(9)
c (Å)	7.6889(5)	7.6852(5)	7.6841(5)
V (Å^3)	228.13(3)	227.90(3)	227.66(3)
χ^2	9.4	2.97	3.49
R_{wp}	3.42	5.55	6.23
R_{Bragg}	10.8	13.3	15.5

Table 2
Structural parameters and magnetic moments for $Nd_{1-x}Sr_xCrO_3$ ($x=0.05$, 0.1 and 0.15) samples at 2 K obtained from the Rietveld analysis of the neutron diffraction data.

Composition	$Nd_{0.95}Sr_{0.05}CrO_3$	$Nd_{0.9}Sr_{0.1}CrO_3$	$Nd_{0.85}Sr_{0.15}CrO_3$
Space group	*Pbnm* (no. 62)		
Nd @ (*x*, *y*, 0.25)			
x	−0.010(2)	−0.009(1)	0.007(2)
y	0.0434(9)	0.037(2)	0.031(1)
B_{iso} (Å)^2	0.05	0.04	0.04
SOF	0.95	0.9	0.85
Cr @ (0.5, 0, 0)			
B_{iso} (Å)^2	0.017	0.017	0.014
SOF	1.0	1.0	1.0
O_1 @ (*x*, *y*, 0.25)			
x	0.060(2)	0.061(1)	0.046(2)
y	0.481(1)	0.484(2)	0.481(2)
B_{iso} (Å)^2	0.02	0.02	0.05
SOF	1.0	1.0	1.0
O_2 @ (*x*, *y*, *z*)			
x	0.714(1)	0.714(3)	0.717(1)
y	0.284(1)	0.291(1)	0.289(1)
z	0.0435(8)	0.0471(8)	0.0499(8)
B_{iso} (Å)^2	0.2	0.2	0.2
SOF	2.0	2.0	2.0
a (Å)	5.4111(9)	5.421(2)	5.419(1)
b (Å)	5.4665(8)	5.4686(9)	5.4667(9)
c (Å)	7.6750(9)	7.682(2)	7.672(1)
V (Å)^3	227.02(6)	227.75(8)	227.28(7)
$\alpha=\beta=\gamma$ (deg)	90	90	90
$\langle\mu_{Cr}\rangle$ (μ_B)	3.19(4)	2.77(3)	2.57(7)
$\mu_{Nd^{3+}}$ (μ_B)	3.0(1)	2.39(8)	2.2(2)
χ^2	1.6	3.81	2.53
R_{wp}	3.98	14.0	18.9
R_{Bragg}	23.8	6.24	4.86
R_{mag} % Cr phase	11.7	13.7	37.0
R_{mag} % Nd phase	36.4	28.4	35.6

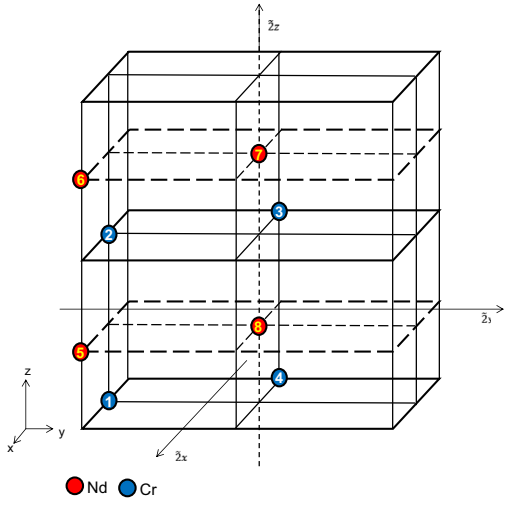

Fig. 4. Typical structure of a $Nd_{1-x}Sr_xCrO_3$sample.

In Fig. 4, a schematic representation of the unit cell of $NdCrO_3$, with only Nd and Cr ions is shown.

For understanding the magnetic structure, we consider the rotation axes, for sake of simplicity, to carry out the independent symmetry analysis on neutron diffraction data. We choose two fold screw axes $\tilde{2}x$ in (x, 1/4, 0), $\tilde{2}y$ in (1/4, y, 1/4) and the inversion center -1 in point 1 as independent symmetry elements [27].

From Fig. 4 for instance, $\tilde{2}x$ sends 1–4 and 2–3; $\tilde{2}y$ sends 4–2 and 3–1. The spin vectors $\mathbf{S}_j$ (j=1,…,8) transform in a complicated way under the operations $\tilde{2}x$, $\tilde{2}y$, and -1 [28]. The linear combinations of Cr spins can be any of the four combinations. The four types of spin arrangements in a magnetic cell can be described as

$$F = S_1 + S_2 + S_3 + S_4 \quad (1a)$$

$$G = S_1 - S_2 + S_3 - S_4 \quad (1b)$$

$$C = S_1 + S_2 - S_3 - S_4 \quad (1c)$$

$$A = S_1 - S_2 - S_3 + S_4 \quad (1d)$$

The pictorial description of the four vectors, which form the basis of irreducible representations, can be shown as in Fig. 5. The spin up and spin down have been shown as filled and open circles, respectively, in the above schematic diagram.

The four representations possible are given as Γ_j (j=1, 2, 3, 4). They are Γ_1 (+++), Γ_2 (+−−), Γ_3 (−++) and Γ_4 (−−+). In our system, we find from the analysis of our neutron diffraction data at 2 K, the Cr atoms moments have a $\mathbf{G_y}$ type of spin alignment. But under the three operations $\tilde{2}x$, $\tilde{2}y$, and -1 the linear combination of spins $\mathbf{G_y}$ does not change sign. So $\mathbf{G_y}$ belongs to (or is a component of) the Γ_1 (+++) representation. It can be easily realized that $\mathbf{A_x}$ and $\mathbf{C_z}$ also transform as Γ_1 (+++). The vector components of the same representation transform identically. In our case, Cr atoms have the $\mathbf{G_y}$ mode and accordingly can admix with $\mathbf{A_x}$ or $\mathbf{C_z}$ as these modes also transform as Γ_1 (+++) representation.

In order to obtain the modes of Nd, it is found that the vector basis of irreducible representations has the same form as for Cr except that the numbering of atoms is 5–8. Working on similar lines, it can be proved that for Nd the three operators $\tilde{2}x$, $\tilde{2}y$, and -1 when operated on the same combinations of spins or basis vectors, give eight distinct irreducible representations. The rise in number of irreducible representations is due to the fact that the operator -1 which sends 5–6 and 7–8 changes the sign of some vector components. The modes of Nd can only be coupled with vectors of the same representation as the modes of Cr which were earlier found to belong to the Γ_1 (+++) representation. This again means only $\mathbf{C_z}$ or $\mathbf{A_x}$ modes of Nd couple with Cr atoms modes. In case of isotropic exchange forces, only one pure mode manifests itself. This theoretical observation is in accordance with our neutron diffraction data analysis (recorded at 2 K) where we find Nd^{3+} ions to have $-\mathbf{C_z}$ modes. In case of anisotropic forces, there can be an admixture of two modes. In our case as we have two modes (one for Cr and one for Nd), we can conclude that there are anisotropic forces at play as is manifested in magnetization.

For both Nd and Cr, the irreducible representations described above were implemented in the Rietveld refinement routine using a propagation vector, k=[0, 0, 0] and the *BasIreps* program in the Fullprof suite.

The average $Cr^{3+/4+}$ ions moment at 2 K was equal to 2.77(3) μ_B for the x=0.1 sample close to its theoretical average of $Cr^{3+/4+}$ moment of 2.85 μ_B. Cr^{3+}–O^{2-}–Cr^{3+}, Cr^{3+}–O^{2-}–Cr^{4+} and Cr^{4+}–O^{2-}–Cr^{4+} superexchange interactions cause alignment of Cr spins. As the valence of Sr^{2+} is not equal to that of Nd^{3+}, 10% of Cr atoms for the x=0.1 sample are in the Cr^{4+} ionic state. The Cr^{4+} ions carry a moment of 2.00(3) μ_B at 2 K equal to its high spin (HS) moment value. The theoretical HS average $Cr^{(3+/4+)}$ moment for x=0.05 sample is 2.9 μ_B while that of the x=0.15 doped sample is 2.7 μ_B. These values are close to our experimental average Cr moments, which are given in Table 2. Therefore, with increasing Sr concentration, the intensities of both the reflection sets (010, 100) and (011, 101) corresponding to only Nd and Nd–Cr interactions, respectively, decrease. This implies that Sr doping leads to a reduction of both Nd–Nd and Nd–Cr couplings. The Nd moments fall with increasing Sr concentration as there is a dilution of the Nd lattice by Sr. A plot of average ⟨Cr⟩ ionic moments as a function of temperature for x=0.10 is shown in Fig. 6. In the inset of Fig. 6, the low angle neutron diffraction patterns of the sample at five different temperatures are shown and the peak near 15.5° representing the Bragg reflections (010) and (100) due to Nd ordering is marked with an arrow. A finite intensity for these reflections at 19 K indicates polarization of Nd moments due to spin reorientation of Cr moments. The Nd^{3+} ions carried a moment of 2.39(8) μ_B at 2 K which is less than the full theoretical moment. The outer electron configuration is $4f^3$ for Nd^{3+} ion. So, its theoretical moment at 0 K (gJ) is 3.27 μ_B. However, the value of Nd^{3+} moment we obtained is within the range of moments for $Nd_{1-x}La_xCrO_3$ from $0 \le x \le 0.9$, namely 2.0 μ_B for x=0.9–2.7 μ_B for x=0.0 [26]. The peak due to Nd–Nd interaction disappears above 19 K.

Fig. 7 is a view of the spin structure at 2 K. The magnetic moments reduce as the temperature rises. The Cr–O_1–Cr and Cr–O_2–Cr angles at 2 K are 159.7° and 152.7°, respectively. Thus, the Cr–O_6 octahedra are tilted as the above mentioned angles have deviated significantly from 180°. Fig. 8 gives a picture of the polyhedra.

From the inset of Fig. 6, we find that the magnetic peaks are absent at 250 K. With increasing temperature, the magnetic contribution to the peaks gets reduced and at 250 K, the purely magnetic peaks due to Cr^{3+}–O^{2-}–Cr^{3+} or Cr^{3+}–O^{2-}–Cr^{4+} and Cr^{4+}–O^{2-}–Cr^{4+} superexchange interactions were not visible. The moments on both Cr^{3+} and Cr^{4+} ions from profile refinement turned out to be close to zero at this temperature. In this scenario, it would be interesting to see how the CrO_6 polyhedra and various

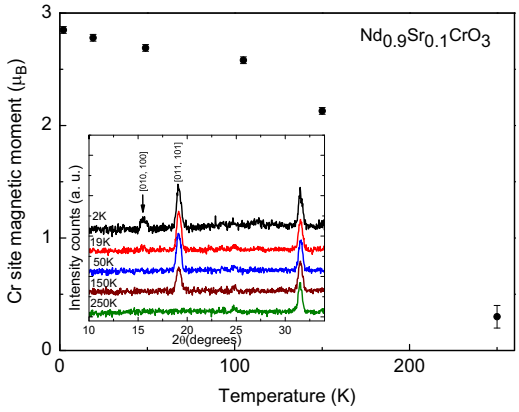

Fig. 6. Average Cr site moment for the x=0.1 sample as a function of temperature. Inset shows low angle diffraction peaks from 2θ=10° to 40° for five different temperatures namely 2 K, 19 K, 50 K, 150 K and 250 K. The arrow shows the finite intensity of the purely magnetic closely spaced (010) and (100) peaks.

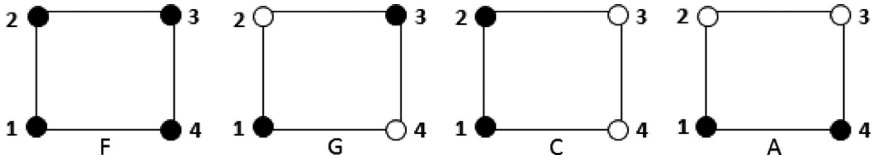

Fig. 5. Pictorial description of the four vectors (F, G, C, and A) which forms the basis of irreducible representations.

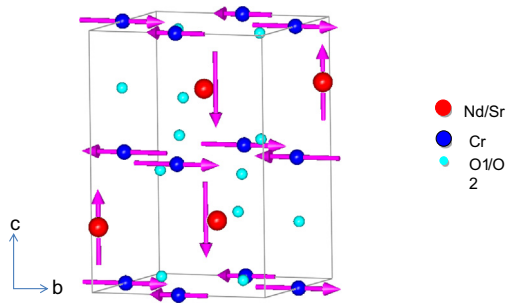

Fig. 7. Pictorial view of spin arrangement in a typical $Nd_{1-x}Sr_xCrO_3$ sample.

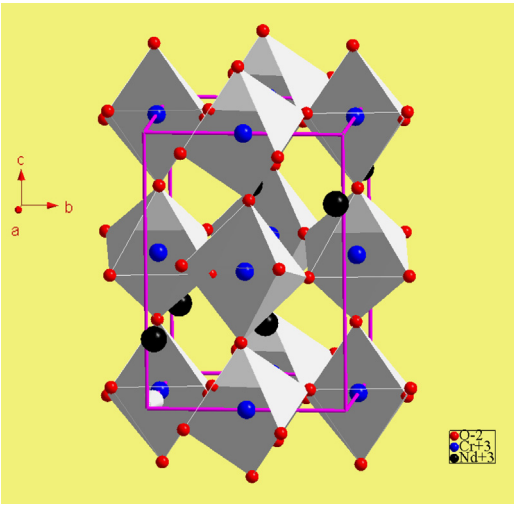

Fig. 8. Pictorial view of tilted $Cr–O_6$ polyhedra in a typical $Nd_{1-x}Sr_xCrO_3$ sample.

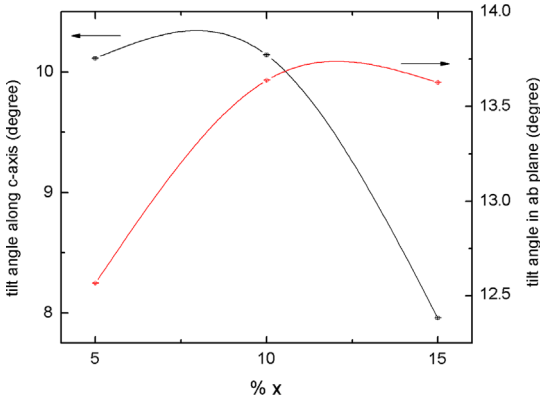

Fig. 9. Tilting in the polyhedra for $Nd_{1-x}Sr_xCrO_3$ (x=0.05, 0.10 and 0.15) is plotted as a function of doping level at 2 K. The titling is calculated using [180−(Cr–O_1–Cr)]/2 and [180−(Cr–O_2–Cr)]/2. Lines joining points are guides to the eye.

Cr–O bond lengths behave as a function of doping at Nd site. Tilt of the polyhedra is calculated by using the expressions [180−(Cr–O_1–Cr)]/2 and [180−(Cr–O_2–Cr)]/2 where Cr–O_1–Cr and Cr–O_2–Cr are axial (along the *c*-axis) and in-plane (in *ab* plane) bond angles [28]. Here Cr–O_1–Cr and Cr–O_2–Cr bond angles and Cr–O_1 and Cr–O_2 bond lengths were calculated by using *BondStr* software in FULLPROF.

Fig. 9 shows the tilting of CrO_6 polyhedra along the *c*-axis and in *ab* plane as a function of doping for $Nd_{1-x}Sr_xCrO_3$ series at 2 K. It is clear from Fig. 9 that tilting along the *c*-axis decreases while that along the *ab* plane increases with respect to increase in Sr doping at Nd site. On close observation, the tilting along *ab* plane

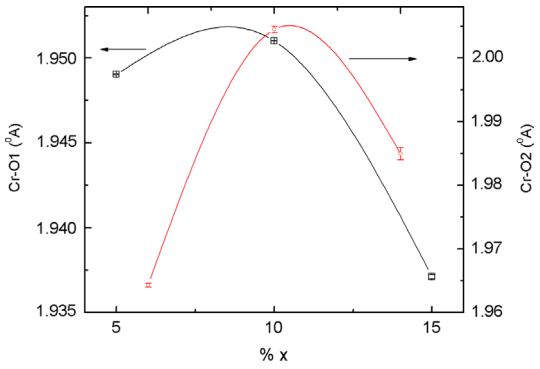

Fig. 10. Cr–O_1 and Cr–O_2 bond lengths for $Nd_{1-x}Sr_xCrO_3$ (x=0.05, 0.10 and 0.15) are plotted as a function of doping level at 2 K. Lines joining points are guide to eye.

decreases for x=0.15 sample, and this decrease in tilting is reflected more clearly in Cr–O_1 and Cr–O_2 bond lengths. In Fig. 10, Cr–O_1 and Cr–O_2 bond lengths along the *c*-axis and *ab* plane, respectively, are plotted as a function of doping level. On systematic doping of Sr at Nd site, Cr–O_1 slightly increases for x=0.1 then decreases further at x=0.15 sample. While for the *ab* plane both Cr–O_1 and Cr–O_2 first increases at x=0.1 and then decrease at x=0.15. This means that the changes observed in the cell parameters due to Sr doping in $NdCrO_3$ can be attributed to the above mentioned changes of bond lengths at the microscopic level.

4. Conclusions

In conclusion, it is observed that $Nd_{1-x}Sr_xCrO_3$ for $0 \le x \le 0.15$ crystallizes in an orthorhombic structure in the temperature range 2–300 K as determined from the detailed temperature dependent neutron diffraction study on these samples. At 2 K, Nd ions have an antiferromagnetic $-\mathbf{C_z}$ type of ordering, while the Cr ions order antiferromagnetically in the $\mathbf{G_y}$ arrangement. These results are in harmony with predictions and experimental results in the literature on $NdCrO_3$ by Shamir et al. [21]. Finite variation in the tilting of CrO_6 polyhedra is observed upon doping of Sr at Nd site which corroborates the magnetic behavior of these samples.

References

[1] D.I. Khomskii, J. Magn. Magn. Mater. 306 (2006) 1;
Y. Tokura, N. Nagaosa, Science 288 (2000) 462;
A.P. Ramirez, J. Phys.: Condens. Matter 9 (1997) 8171.
[2] J. van den Brink, D.I. Khomskii, J. Phys.: Condens. Matter 20 (2008) 434217.
[3] G.V. Subba Rao, G.V. Chandrashekhar, C.N.R. Rao, Solid State Commun. 6 (1968) 177.
[4] H.B. Lal, R.D. Dwivedi, K.J. Gaur, J. Mater. Sci. – Mater. Electron. 7 (1996) 35.
[5] J.R. Sahu, C.R. Serrao, N. Ray, U.V. Waghmare, C.N.R. Rao, J. Mater. Chem. 17 (2007) 42.
[6] A. Zvezdin, A. Mukhin, JETP Lett. 88 (2008) 505.
[7] Z.X. Cheng, X.L. Wang, S.X. Dou, H. Kimura, K. Ozawa, J. Appl. Phys. 107 (2010) 09D905.
[8] R. Raffaelle, H.U. Anderson, D.M. Sparlin, P.E. Parris, Phys. Rev. Lett. 65 (1990) 1383.
[9] G.A. Tompsett, N.M. Sammes, J. Power Sources 130 (2004) 1.
[10] J.J. Kingsley, L.R. Pederson, Mater. Lett. 18 (1993) 89.
[11] V.F. Savchenko, Y.S. Rubinchik, Neorg. Mater. 15 (1979) 122.
[12] A. Galdón, M.C. Guillem, Solid State Ion. 63 (1993) 66.
[13] G.J. McCarthy, P.V. GallagherC. Sipe, Mater. Res. Bull. 8 (1973) 1277.
[14] S.S. Manoharan, K.C. Patil, J. Solid State Chem. 102 (1993) 267.
[15] A.K. Tripathi, J. Am. Ceram. Soc. 63 (1980) 475.
[16] A.K. Tripathi, H.B. Lal, J. Mater. Sci. 17 (1982) 1595.
[17] S.F. Palguev, V.I. Zemtzov, V.K. Gilderman, A.D. Neujmin, Solid State Ion. 13 (1984) 65.
[18] D.P. Karim, A.T. Aldred, Phys. Rev. B 20 (1979) 2255.
[19] W.J. Weber, C.W. Griffin, J.L. Bates, J. Am. Ceram. Soc. 70 (1987) 265.
[20] Liu Monan, Yu Shen, Ji Yuan, He Tianmin, J. Alloys. Compd. 461 (2008) 628.

[21] N. Shamir, H. Shaked, S. Shtrikman, Phys. Rev. B 24 (1981) 6642.
[22] E.F. Bertaut, J. Mareschal, G. De Vries, R. Algonard, R. Pauthenet, J.P. Rebouillat, V. Zarubicka, IEEE Trans. Magn. 2 (1966) 453.
[23] Juan Rodriguez-Carvajal, Physica B 192 (1993) 55.
[25] E.F. Bertaut, J. Mareschal, Solid State Commun. 5 (1967) 93.
[26] Yi Du, Xiang Cheng Zhen, Xiao-Lin Wang, Shi Xue Dou, J. Appl. Phys. 108 (2010) 93914.
[27] E.F. Bertaut, in: G.T. Rado, H. Suhl (Eds.), Magnetism, vol. 3, Academic Press Inc., London, 1963, pp. 150–209.
[28] Keka R. Chakraborty, S.M. Yusuf, P.S.R. Krishna, M. Ramanadham, V. Pomjakushin, A.K. Tyagi, J. Phys.: Condens. Matter 19 (2007) 216207.

Further reading

[24] R.M. Hornreich, Y. Komet, R. Nolan, B.M. Wanklyn, I. Yaeger, Phys. Rev. B 12 (1975) 5094.